Improved Photocatalytic Hydrogen Evolution on Tantalate Perovskites CsTaO 3 and LiTaO 3 by Strain-Induced Vacancies

Kaveh Edalati, Keisuke Fujiwara, Shuhei Takechi, Qing Wang, Makoto Arita, Motonori Watanabe, Xavier Sauvage, Tatsumi Ishihara, Zenji Horita

Enhanced Photocatalytic Hydrogen Production on Tantalate Perovskites $CsTaO_3$ and $LiTaO_3$ by Strain-Induced Vacancies

Kaveh Edalati[1,2,*], Keisuke Fujiwara[1,2], Shuhei Takechi[3], Qing Wang[1], Makoto Arita[2], Motonori Watanabe[1], Xavier Sauvage[4], Tatsumi Ishihara[1,3] and Zenji Horita[1,2]

[1] WPI, International Institute for Carbon-Neutral Energy Research (WPI-I2CNER), Kyushu University, Fukuoka, Japan
[2] Department of Materials Science and Engineering, Faculty of Engineering, Kyushu University, Fukuoka, Japan
[3] Department of Applied Chemistry, Faculty of Engineering, Kyushu University, Fukuoka, Japan
[4] Normandie Université, UNIROUEN, INSA Rouen, CNRS, Groupe de Physique des Matériaux, 76000 Rouen, France

Tantalate perovskites are considered as potential candidates for photocatalytic hydrogen production because their electronic band structure satisfies the requirements for water splitting. However, these oxides have large bandgaps which results in their low photocatalytic activity. In this study, to enhance the photocatalytic activity of tantalate perovskites, $CsTaO_3$ as a new photocatalyst is mechanically subjected to severe plastic strain of $\varepsilon \geq 13$ using the high-pressure torsion (HPT) method and its performance is compared with $LiTaO_3$. Both super-strained tantalates exhibit bandgap narrowing together with decreasing the conduction band energy with similar enhancement of the photocatalytic hydrogen production (by a factor of ~2.5 without cocatalyst addition). Such bandgap narrowing is mainly due to the formation of oxygen vacancies and lattice straining, although the formation of nanocrystals and partial amorphization also occur. These findings not only introduce $CsTaO_3$ as a photocatalyst but also confirm that the production of strain-induced vacancies is an effective approach to improve the photocatalytic activity of perovskites.

Keywords: Photocatalysis; Lithium tantalate; Cesium tantalate; Oxygen vacancy; Severe plastic deformation (SPD); High-pressure torsion (HPT)

*Corresponding author (E-mail: kaveh.edalati@kyudai.jp; Tel: +81 92 802 6735)

Introduction

Phototocatalysis is considered as an efficient method to harvest solar energy for promoting particular chemical reactions in the presence of a non-metallic catalyst [1]. These catalysts, i.e. photocatalysts, are mainly semiconductor oxides which can produce photo-induced electron and holes for chemical reactions [1]. High interest on photocatalysis was initiated with a study on photo-induced water splitting on TiO_2, which suggested a new approach for clean production of hydrogen [2]. Since photocatalysis is principally applicable to control some critical reactions such as water splitting or conversion of carbon dioxide to hydrocarbons, there are now significant activities all around the word not only to discover new photocatalysts but also to find new methods to improve the performance of existing photocatalysts [3,4].

Tantalate perovskites have been widely investigated for photocatalytic hydrogen production because their electronic band structure satisfies the requirements for water splitting, i.e. their valence band energy is more negative than -5.6 eV for H_2O/O_2 conversion and their conduction band energy is more positive than -4.4 eV for H^+/H_2 conversion [5-7]. Among these perovskites, alkali tantalate perovskites such as $LiTaO_3$, $NaTaO_3$ and $KTaO_3$ have received significant attention because they can decompose water without any need of a cocatalyst or scavenger [8,9], while water splitting on TiO_2 usually needs Pt as a cocatalyst and methanol as a scavenger [10].

Despite the significant advantage of alkali tantalate perovskites for water splitting without cocatalyst [8,9], their main drawback is their high bandgap which reduces their photocatalytic activity: 4.7 eV for $LiTaO_3$, 4.0 eV for $NaTaO_3$ and 3.6 for $KTaO_3$ [5,11]. Although the trend of bandgap for alkali tantalate perovskites suggests that the bandgap decreases with increasing the atomic number of alkali element [5,11], there have been no attempt to use $CsTaO_3$ for photoacatlysis. So far, different approaches were employed to enhance the photocatalytic activity of $LiTaO_3$, $NaTaO_3$ and $KTaO_3$: atomic doping with other elements [12-15], making composites [16-18] and amorphization of crystal structure [19,20]. Despite these attempts, the photocatalytic activity of these materials still need to be improved by exploring new strategies. Here, strain-induced oxygen vacancy generation is introduced as a new strategy for such an improvement.

In this study, to improve the photocatalytic activity of alkaline tantalate perovskites, severe plastic strain is introduced into the materials using a mechanical process, so-called high-pressure torsion (HPT) [21-23]. Moreover, $CsTaO_3$ is investigated as a photocatalyst for the first time and its performance is compared with widely-investigated $LiTaO_3$. It is found that straining by HPT is quite effective to reduce the bandgap and improve the photocatalytic activity of both $CsTaO_3$ and $LiTaO_3$. It should be noted that although, the HPT method is mainly used as a severe plastic deformation (SPD) method for producing nanograined phases in metallic [24-26] and nonmetallic [27-29] materials. However, a few studies showed the potential of the method for producing high-pressure or highly-strained oxide phases with large oxygen vacancy concentration and enhanced photocatlytic activity such as columbite-TiO_2 [30], rocksalt-ZnO [31], columbite-TiO_2 / rocksalt-ZnO composite [32] and defected α-Al_2O_3 [33].

Experimental Procedures

The materials used in this study were powders of high-purity (99.9%) $CsTaO_3$ and $LiTaO_3$ with the orthorhombic (space group: pbam, a = 2.622 nm, b = 0.743 nm, c = 0.739 nm, $\alpha = \beta = \gamma = 90^o$ [34]) and rhombohedral (space group: R3c, $a = b$ = 5.154, c = 1.377, $\alpha = \beta = 90^o$, $\gamma = 120^o$ [35]) crystal structures, respectively. For the introduction of strain, ~0.5 g of the powders were

processed between two HPT anvils under a pressure of 6 GPa at ambient temperature by rotating the lower HPT anvil with respect to the upper one for 1 turn with a rotation speed of 1 rpm. The HPT anvils were made of tungsten carbide - cobalt composites, in which the flat-bottom holes with 10 mm diameter and 0.25 mm depth were machined on the surfaces. The imposed strain was a function of distance from the disc center and was calculated as $\varepsilon = 2\pi rN/\sqrt{3}h$ (ε: von-Mises equivalent strain; r: distance from disc center, N: number of turns, h: thickness of disc which was ~0.8 mm) [21]. After HPT processing, the super-strained edge area of the disc samples ($r \geq 3$ mm or $\varepsilon \geq 13$) were examined by different techniques.

First, the phase transformations were examined by X-ray diffraction (XRD) analysis using Cu Kα radiation and by Raman spectroscopy using a He-Cd laser source with 325 nm wavelength.

Second, the microstructure of samples was examined by an aberration-corrected transmission electron microscope under an acceleration voltage of 200 kV using the high-resolution imaging mode, selected-area electron diffraction (SAED) and electron energy loss spectroscopy (EELS). Thin foils for TEM were prepared by crushing the edge of samples and pouring them onto carbon grids.

Third, formation of oxygen vacancies was examined by X-ray photoelectron spectroscopy (XPS) using a Mg Kα X-ray source, by photoluminescence (PL) measurement using a He-Cd laser source with 325 nm wavelength and by electron spin resonance (EPR) with a 9468.8 MHz microwave source operated at 298 K.

Fourth, the optical bandgap was estimated by UV-Vis (ultraviolet-visible light) diffuse reflectance spectroscopy and by employing the Kubelka-Munk method.

Fifth, the energy level for the top of valence band (E_V) was estimated by ultraviolet photoelectron spectroscopy (UPS) using a He UV light source under an electrical bias of 5 V. Accordingly, the energy level for the bottom of conduction band (E_C) was calculated as optical bandgap (E_g) plus energy level at the top of valence band, $E_C = E_V + Eg$.

Sixth, the photocatalytic activity of perovskites was evaluated for water splitting using a 300 W Hg lamp by addition of 50 mg of crushed powders to 30 mL H_2O without addition of any cocatalyst or scavenger.

Results and Discussion

Examination of phase transformations by XRD and Raman spectroscopy, as shown in Fig. 1, confirms that no phase transformations occur in $CsTaO_3$ and $LiTaO_3$ by HPT processing. However, a clear peak broadening appears after HPT processing, indicating the occurrence of lattice strain by the formation of lattice defects and crystallite size reduction. The increase in the intensity of Raman background also suggests the formation of lattice defects (Figs. 1(c) and (d)). It should be noted that the occurrence of phase transformation was examined by EELS, but no clear evidence for phase transformation was found, as shown in Fig. A1. Taken altogether, unlike other investigated oxides such as ZrO_2 [36], $BaTiO_3$ [37], TiO_2 [30,38], ZnO [31], VO_2 [39] and Al_2O_3 [33,40] in which phase transformations occurred by HPT processing, no phase transformations in the crystalline form are detectable in the HPT-processed $CsTaO_3$ and $LiTaO_3$.

Detailed structural analysis using TEM, as shown in Fig. 2, reveals several important points. First, SAED patterns are typical of large single crystal domains before HPT processing, but they exhibit Debbye-Scherrer rings typical of nanocrystals after HPT processing. This indicates that small nanograins with random orientations are developed during HPT processing. Second, in the SAED pattern of $CsTaO_3$, halo-shaped rings appear after HPT processing, which indicates the

occurrence of partial amorphization in this material. Third, examination of microstructure of $LiTaO_3$ by high-resolution TEM confirms the presence of large defect-free grains prior to deformation, while nanograin boundaries appear clearly after HPT processing, as shown in Fig. 2(d). Fourth, micrograins transform to the nangrained and amorphous regions in $CsTaO_3$ by HPT processing, as shown in Fig. 2(b), while amorphization in $LiTaO_3$ was negligible compared with $CsTaO_3$. Fifth, the average grain size for both materials after HPT processing is ~40 nm (excluding the amorphous regions). The occurrence of grain refinement by HPT processing is a natural consequence of plastic strain effect, which was reported in various metallic [24-26] and nonmetallic [27-29] materials. Moreover, HPT-induced partial amorphization is not a rare phenomenon as it was reported in several materials especially intermetallics and multicomponent alloys [41], although HPT-induced partial crystallization was also reported in some amorphous alloys [42].

To examine the formation of points defects and particularly oxygen vacancies, ESR and PL examinations were conducted, as shown in Fig. 3. ESR shows the presence of peaks at *g* value of ~2, which usually corresponds to the presence of oxygen vacancies and Ta^{+4} in alkali tantalate perovskites [43,44]. Although ESR confirms the presence of oxygen vacancies before and after HPT processing, it does not provide a clear evidence for the change of oxygen vacancy concentration after HPT processing. PL spectra show the presence of two intense peaks at ~400 nm and ~530 nm after HPT which is consistent the PL peak positions reported in defected alkali tantalate perovskites [44,45]. These PL peaks correspond to the formation of oxygen vacancies and Ta^{+4} [44]. It should be noted that XPS spectra, as shown in Fig. A2, provide no clear evidence for oxygen vacancy generation probably because the concentration of vacancies is below the detection limits of XPS. It is then concluded that HPT processing can induce oxygen vacancies in $CsTaO_3$ and $LiTaO_3$ in good agreement with the earlier reports on the formation of oxygen vacancies in the HPT-processed $BaTiO_3$ [37], TiO_2 [30], ZnO [31], Al_2O_3 [33,40] and TiO_2-ZnO [32]. The formation of vacancies by HPT processing is due to the strain effect on continuous generation of vacancies and the pressure effect on suppressing the migration and annihilation of vacancies [46-48].

The influence of HPT processing on the light absorbance and optical bandgap is shown in Fig. 4 using the UV-vis spectroscopy. Examination of Fig. 4 indicates several important points. First, the UV-vis spectra in Figs. 4(a) and (b) show that both oxides exhibit better light absorbance with an extended tail absorbance to the visible light region after HPT processing. The tail absorbance in the visible light region can be attributed to the formation of localized oxygen vacancy states between the valence band and conduction band [49]. Second, estimation of the optical bandgap using the Kubelka-Munk method [50], as shown in Figs. 4(c) and (d), confirms that both materials exhibit similar optical bandgap before HPT processing. Although it is empirically expected that bandgap decreases with increasing the atomic number of alkali element in the tantalate perovskites (4.7 eV for $LiTaO_3$, 4.0 eV for $NaTaO_3$ and 3.6 for $KTaO_3$ [5,11]), $CsTaO_3$ does not follow this trend and show a high bandgap as 4.6 eV, perhaps because of its different atomic arrangement in the form of orthorhombic crystal structure. Third, the bandgap is reduced in both oxides after straining. Fourth, in addition to the slope corresponding to the optical bandgap, two other slopes with energy levels of 2.5 eV and 3-3.2 eV appear in the Kubelka-Munk plots after HPT processing. These slopes, which are reasonably consistent with the energy levels for the PL spectra in Fig. 3, should be due to formation of oxygen vacancy states in the bandgap. Taken altogether, decreasing the bandgap of $CsTaO_3$ and $LiTaO_3$ by straining via the HPT process together with earlier reports on decreasing the bandgap in TiO_2 [30], ZnO [31], Al_2O_3 [33,40] and

TiO_2-ZnO [32] by HPT processing, demonstrate that the HPT method as an effective route for bandgap narrowing of photocatalysts.

Since the energy levels for the valence and conduction bands are critical factors for photocatalytic water splitting, the energy levels were examined by UPS combined with UV-vis spectroscopy, as attempted earlier [51]. Examination of the UPS spectra, as shown in Figs. 5(a) and (b), shows the energy level for the top of valence band in $CsTaO_3$ increases from -6.4 eV to -6.0 eV after HPT processing, but a constant energy level of -6.8 eV is achieved in $LiTaO_3$ before and after processing by HPT. A simple calculation assuming that $E_C = E_V + Eg$ demonstrates that the conduction band energy decreases by HPT processing from -1.8 eV to -2.3 eV for $CsTaO_3$ and from -2.1 eV to -2.6 eV for $LiTaO_3$. Here, it should be noted that the bandgap and the valence band energy levels achieved in this study for $LiTaO_3$ powder are consistent with those reported earlier in the literature [5-7]. Although, theoretical calculations predicated a bandgap in the range of 2.9 to 3.7 eV for $CsTaO_3$ [52,53], there have been no experimental data to be compared with the measured bandgap in this study. As summarized in Figs. 5(b) and (d), the electronic structures of both $CsTaO_3$ and $LiTaO_3$ before and after processing by HPT satisfy the required conditions for photocatalytic hydrogen production, i.e. the valence band energy is more negative than -5.6 eV (energy level for the reduction of H^+ to H_2) and the conduction band energy is more positive than -4.4 eV (energy level for conversion of H_2O to O_2) [51].

To examine the photocatalytic activity of $CsTaO_3$ and $LiTaO_3$, photocatalytic water splitting was conducted without addition of any cocatalyst or scavenger. As shown in Fig. 6, photocatalytic hydrogen production on both materials is enhanced after processing by HPT. Moreover, $CsTaO_3$ and $LiTaO_3$ show similar photocatalytic activity, especially before processing by HPT. It is then concluded that $CsTaO_3$ can be considered as a new photocatalyst which can decompose water without any need to co-catalyst and scavenger, while most of the photocatalysts such as TiO_2 need cocatalyst and scavenger addition [2,10]. Another important issue is that super-straining by HPT not only reduces the bandgap but also improve the photocatalytic activity by producing the active sites for photocatalysis such as oxygen vacancies or highly-defected regions. It should be noted that other approaches employed so far to enhance the photocatalytic activity of alakali tantalate perovskites such as atomic doping with other elements [12-15], making composites [16-18] and amorphization of crystal structure [19,20] are all based on chemical methods, while the HPT method is a mechanical method which can enhance the photocatalytic activity of even pure tantalates.

Conclusions

In this study, $CsTaO_3$ as a new photocatalyst and $LiTaO_3$ as a highly-investigated photocatalyst were subjected to super straining using the high-pressure torsion (HPT) method and their microstructure, optical properties and photocatalytic activity were investigated. The oxides transformed mainly to naongrains and partly into amorphous regions with large fraction of oxygen vacancies after super-straining. Such microstructural changes resulted in bandgap narrowing and enhancement of photocatalytic hydrogen evolution. These findings introduce a simple but effective approach to enhance the photocatalytic activity of perovskites.

Acknowledgments

This work is supported in part by WPI-I2CNER, Japan, and in part by Grants-in-Aid for Scientific Research from MEXT, Japan (16H04539 & 26220909). The HPT process was carried

out in IRC-GSAM at Kyushu University. TEM experiments were carried out on a GENESIS facility, supported by the Région Normandie, France, and by the French National Research Agency (ANR-11-EQPX-0020).

Appendix

Additional experiments were conducted using the EELS and XPS techniques to examine the phase transformation and oxygen vacancy generation. As shown in Fig. A1, the EELS spectra in both low-loss and high-loss modes show no significant changes after HPT processing, suggesting the absence of phase transformation after processing. The XPS spectra in Fig. A2 also reveal no appreciable changes after processing, indicating that the concentration of oxygen vacancies is not so high to be detected by XPS.

References

[1] M.R. Hoffmann, S.T. Martin, W. Choi, D.W. Bahnemann, Environmental applications of semiconductor photocatalysis, Chem. Rev. 95 (1995) 69-96.
[2] A. Fujishima, K. Honda, Electrochemical photolysis of water at a semiconductor electrode, Nature 238 (1972) 37-38.
[3] H. Tong, S. Ouyang, Y. Bi, N. Umezawa, M. Oshikiri, J. Ye, Nano-photocatalytic materials: possibilities and challenges, Adv. Mater. 24 (2012) 229-251.
[4] D.M. Schultz, T.P. Yoon, Solar synthesis: prospects in visible light photocatalysis, Science 343 (2014) 1239176.
[5] H. Kato, A. Kudo, New tantalate photocatalysts for water decomposition into H_2 and O_2, Chem. Phys. Lett. 295 (1998) 487-492.
[6] A. Kudo, Y. Miseki, Heterogeneous photocatalyst materials for water splitting, Chem. Soc. Rev. 38 (2009) 253-278.
[7] P. Zhang, J. Zhang, J. Gong, Tantalum-based semiconductors for solar water splitting, Chem. Soc. Rev. 43 (2014) 4395-4422.
[8] S. Takasugi, K. Tomita, M. Iwaoka, H. Kato, M. Kakihana, The hydrothermal and solvothermal synthesis of $LiTaO_3$ photocatalyst: suppressing the deterioration of the water splitting activity without using a cocatalyst, Int. J. Hydrogen Energy 40 (2015) 5638-5643.
[9] S. Zlotnik, D.M. Tobaldi, P. Seabra, J.A. Labrincha, P.M. Vilarinho, Alkali niobate and tantalate perovskites as alternative photocatalysts, ChemPhysChem 17 (2016) 3570-3575.
[10] A. Fujishima, T.N. Rao, D.A. Tryk, Titanium dioxide photocatalysis, J Photoch. Photobio. C 1 (2000) 1-21.
[11] A. Kudo, H. Kato, I. Tsuji, Strategies for the development of visible-light-driven photocatalysts for water splitting, Chem. Lett. 33 (2004) 1534-1539.
[12] T. Ishihara, H. Nishiguchi, K. Fukamachi, Y. Takita, Effects of acceptor doping to $KTaO_3$ on photocatalytic decomposition of pure H_2O, J. Phys. Chem. B 103 (1999) 1-3.
[13] P.D. Kanhere, J. Zheng, Z. Chen, Site specific optical and photocatalytic properties of Bi-doped $NaTaO_3$, J. Phys. Chem. C 115 (2011) 11846-11853.
[14] B. Wang, P.D. Kanhere, Z. Chen, J. Nisar, B. Pathak, R. Ahuja, Anion-doped $NaTaO_3$ for visible light photocatalysis, J. Phys. Chem. C 117 (2013) 22518-22524.
[15] F.F. Li, D.R. Liu, G.M. Gao, B. Xue, Y.S. Jiang, Improved visible-light photocatalytic activity of $NaTaO_3$ with perovskite-like structure via sulfur anion doping, Appl. Catal. B 166–167 (2015) 104-111.

[16] B. Bajorowicz, J. Nadolna, W. Lisowski, T. Klimczuk, A. Zaleska-Medynska, The effects of bifunctional linker and reflux time on the surface properties and photocatalytic activity of CdTe quantum dots decorated $KTaO_3$ composite photocatalysts, Appl. Catalysis B 203 (2017) 452-464.
[17] D. Xu, W. Shi, C. Song, M. Chen, S. Yang, W. Fan, B. Chen, In-situ synthesis and enhanced photocatalytic activity of visible-light-driven plasmonic Ag/AgCl/$NaTaO_3$ nanocubes photocatalysts, Appl. Catal. B 191 (2016) 228-234.
[18] D. Xu, M. Chen, S. Song, D. Jiang, W. Fan, W. Shi, The synthesis of a novel Ag-$NaTaO_3$ hybrid with plasmonic photocatalytic activity under visible-light, CrystEngComm 16 (2014) 1384-1388.
[19] H. Tüysüz, C.K. Chan, Preparation of amorphous and nanocrystalline sodium tantalum oxide photocatalysts with porous matrix structure for overall water splitting, Nano Energy 2 (2013) 116-123.
[20] T. Grewe, H. Tuysuz, Amorphous and crystalline sodium tantalate composites for photocatalytic water splitting, ACS Appl. Mater. Interfaces 7 (2015) 23153-23162.
[21] R.Z. Valiev, Y. Estrin, Z. Horita, T.G. Langdon, M.J. Zehetbauer, Y.T. Zhu, Producing bulk ultrafine-grained materials by severe plastic deformation, JOM 58(4) (2006) 33-39.
[22] A.P. Zhilyaev, T.G. Langdon, Using high-pressure torsion for metal processing: fundamentals and applications, Prog. Mater. Sci. 53 (2008) 893-979.
[23] K. Edalati, Z. Horita, A review on high-pressure torsion from 1935 to 1988. Mater. Sci. Eng. A 652 (2016) 325-352.
[24] A. Bachmaier, R. Pippan, High-pressure torsion deformation induced phase transformations and formations: new material combinations and advanced properties, Mater. Trans. 60 (2019) 1256-1269.
[25] J.K. Han, J.I. Jang, T.G. Langdon, M. Kawasaki, Bulk-state reactions and improving the mechanical properties of metals through high-pressure torsion, Mater. Trans. 60 (2019) 1131-1138.
[26] V.V. Popov, E.N. Popova, Behavior of Nb and CuNb composites under severe plastic deformation and annealing, Mater. Trans. 60 (2019) 1209-1220.
[27] K. Edalati, Review on recent advancement in severe plastic deformation of oxides by high-pressure torsion (HPT), Adv. Eng. Mater. 21 (2019) 1800272.
[28] V.D. Blank, M.Y. Popov, B.A. Kulnitskiy, The effect of severe plastic deformations on phase transitions and structure of solids, Mater. Trans. 60 (2019) 1500-1505.
[29] V.I. Levitas, High-pressure phase transformations under severe plastic deformation by torsion in rotational anvils, Mater. Trans. 60 (2019) 1294-1301.
[30] H. Razavi-Khosroshahi, K. Edalati, M. Hirayama, H. Emami, M. Arita, M. Yamauchi, H. Hagiwara, S. Ida, T. Ishihara, E. Akiba, Z. Horita, M. Fuji, Visible-light-driven photocatalytic hydrogen generation on nanosized TiO_2-II stabilized by high-pressure torsion, ACS Catal.6 (2016) 5103-5107.
[31] H. Razavi-Khosroshahi, K. Edalati, J. Wu, Y. Nakashima, M. Arita, Y. Ikoma, M. Sadakiyo, Y. Inagaki, A. Staykov, M. Yamauchi, Z. Horita, M. Fuji, High-pressure zinc oxide phase as visible-light-active photocatalyst with narrow band gap, J. Mater. Chem. A 5 (2017) 20298-20303.
[32] J. Hidalgo-Jimenez, Q. Wang, K. Edalati, J. Cubero-Sesin, H. Razavi-Khosroshahi, Y. Ikoma, D. Gutierrez-Fallas, F.A. Dittel-Meza, J.C. Rodriguez-Rufino, M. Fuji, Z. Horita, High-

pressure torsion of TiO_2-ZnO composites: phase transformations, vacancy formation and changes in optical and photocatalytic properties, Int. J. Plasticity (2019) in press.
[33] K. Edalati, I. Fujita, S. Takechi, Y. Nakashima, K. Kumano, H. Razavi-Khosroshahi, M. Arita, M. Watanabe, X. Sauvage, T. Akbay, T. Ishihara, M. Fuji, Z. Horita, Photocatalytic activity of aluminum oxide by oxygen vacancy generation using high-pressure torsion straining, Scr. Mater. 173 (2019) 120-124.
[34] N. Ishizawa, A. Oono, D. du Boulay, A reinvestigation of the structure of $Cs_3Ta_5O_{14}$, Acta Crystallogr. E 59 (2003) i86-i88.
[35] T.V. Tkachenko, E.I. Get'man, S.K. Bamoteref, $LiTaO_3$-$SrZrO_3$ system, Russ. J. Inorg. Chem. 36 (1991) 1645-1647.
[36] K. Edalati, S. Toh, Y. Ikoma, Z. Horita, Plastic deformation and allotropic phase transformations in zirconia ceramics during high-pressure torsion, Scr. Mater. 65 (2011) 974-977.
[37] K. Edalati, M. Arimura, Y. Ikoma, T. Daio, M. Miyata, D.J. Smith, Z. Horita, Plastic deformation of $BaTiO_3$ ceramics by high-pressure torsion and changes in phase transformations, optical and dielectric properties. Mater. Res. Lett. 3 (2015) 216-221.
[38] K. Edalati, Q. Wang, H. Razavi-Khosroshahi, H. Emami, M. Fuji, Z. Horita, Low-temperature anatase-to-rutile phase transformation and unusual grain coarsening in titanium oxide nanopowders by high-pressure torsion straining, Scr. Mater. 162 (2019) 341-344.
[39] K. Edalati, I. Fujita, X. Sauvage, M. Arita, Z. Horita, Microstructure and phase transformations of silica glass and vanadium oxide by severe plastic deformation via high-pressure torsion straining, J. Alloys Compd. 779 (2019) 394-398.
[40] I. Fujita, K. Edalati, X. Sauvage, Z. Horita, Grain growth in nanograined aluminum oxide by high-pressure torsion: phase transformation and plastic strain effects, Scr. Mater. 152 (2018) 11-14.
[41] A. Mazilkin, B. Straumal, A. Kilmametov, P. Straumal, B. Baretzky, Phase transformations induced by severe plastic deformation, Mater. Trans. 60 (2019) 1489-1499.
[42] Á. Révész, Z. Kovács, Severe plastic deformation of amorphous alloys, Mater. Trans. 60 (2019) 1283-1293.
[43] J.Q. Wang, S.Y. Su, B. Liu, M.H. Cao, C.W. Hu, One-pot, low-temperature synthesis of self-doped $NaTaO_3$ nanoclusters for visible-light-driven photocatalysis, Chem. Commun. 49 (2013) 7830-7832.
[44] J. Hou, S. Cao, Y. Wu, F. Liang, L. Ye, Z. Lin, L. Sun, Perovskite-based nanocubes with simultaneously improved visible-light absorption and charge separation enabling efficient photocatalytic CO_2 reduction, Nano Energy 30 (2016) 59-68.
[45] Y.C. Lee, H. Teng, C.C. Hu, S.Y. Hu, Temperature-dependent photoluminescence in $NaTaO_3$ with different crystalline structures, Electrochem. Solid-State Lett. 11 (2008) P1-P4.
[46] B. Oberdorfer, B. Lorenzoni, K. Unger, W. Sprengel, M. Zehetbauer, R. Pippan R. Wurschum, Absolute concentration of free volume-type defects in ultrafine-grained Fe prepared by high-pressure torsion, Scr. Mater. 63 (2010) 452-455.
[47] M. Krystian, D. Setman, B. Mingler, G. Krexner, M.J. Zehetbauer, Formation of superabundant vacancies in nano-Pd-H generated by high-pressure torsion, Scr. Mater. 62 (2010) 49-52.
[48] J. Čížek, M. Janeček, T. Vlasák, B. Smola, O. Melikhova, R.K. Islamgaliev, S.V. Dobatkin, The development of vacancies during severe plastic deformation, Mater. Trans. 60 (2019) 1533-1542.

[49] S. John, C. Soukoulis, M.H. Cohen, E.N. Economou, Theory of electron band tails and the Urbach optical-absorption edge, Phys. Rev. Lett. 57 (1986) 1777-1780.
[50] P. Kubelka, F. Munk, An article on optics of paint layers, Zeit. Fur Teken Physik 12 (1931) 593-601.
[51] W.J. Chun, A. Ishikawa, H. Fujisawa, T. Takata, J.N. Kondo, M. Hara, M. Kawai, Y. Matsumoto, K. Domen, Conduction and valence band positions of Ta_2O_5, TaON, and Ta_3N_5 by UPS and electrochemical methods, J. Phys. Chem. B 107 (2003) 1798-1803.
[52] I.E. Castelli, J.M. García-Lastra, F. Hüser, K.S. Thygesen, K.W. Jacobsen, Stability and bandgaps of layered perovskites for one- and two-photon water splitting, New J. Phys. 15 (2013) 105026.
[53] B. Sabir, G. Murtaza, R.M. Arif Khalil, Qasim Mahmood, First principle study of electronic, mechanical, optical and thermoelectric properties of $CsMO_3$ (M = Ta, Nb) compounds for optoelectronic devices, J. Mol. Graph. Model. 86 (2019) 19-26.

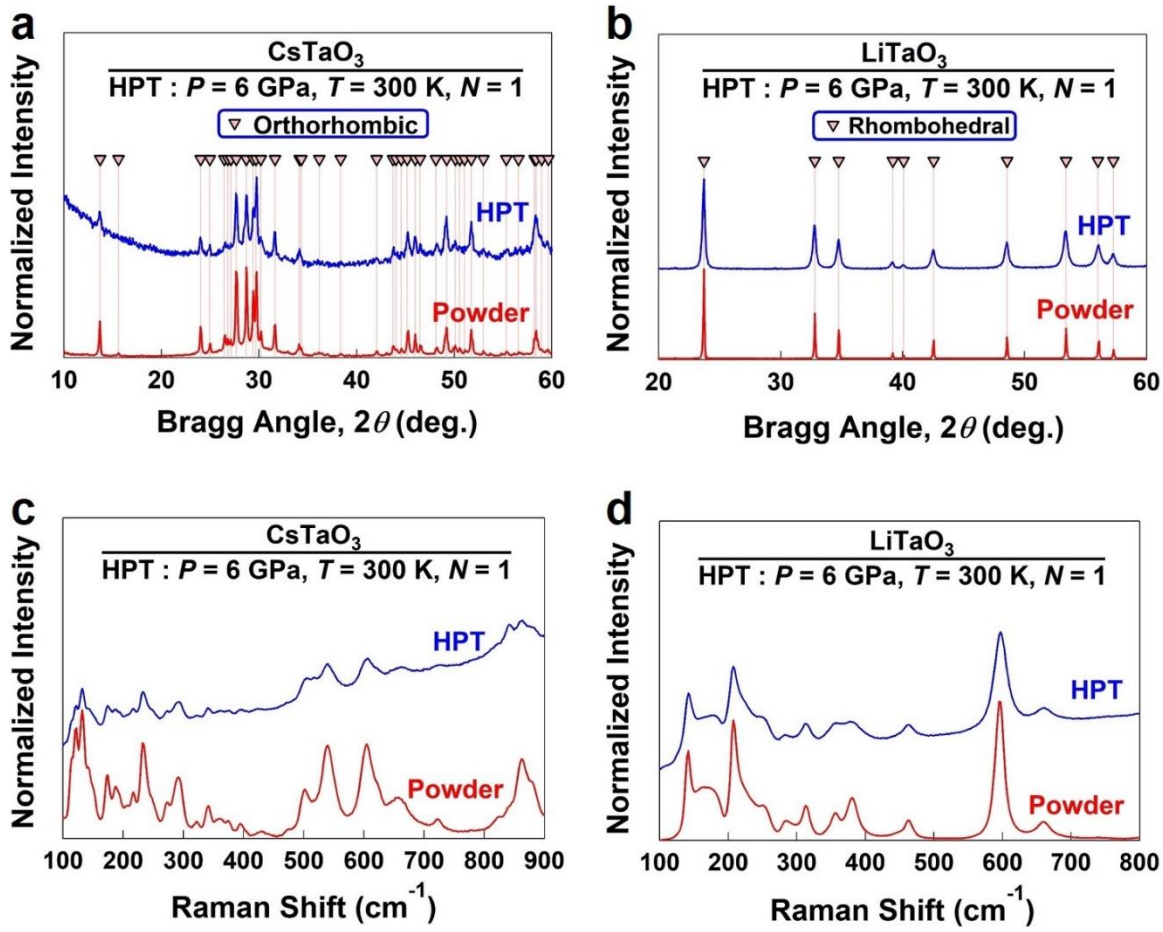

Figure 1. Formation of lattice defects without phase transformation to crystalline form in tantalate perovskites by severe straining. (a, b) XRD profiles and (c, d) Raman spectra for (a, c) $CsTaO_3$ and (b, d) $LiTaO_3$ before (powder) and after processing by HPT.

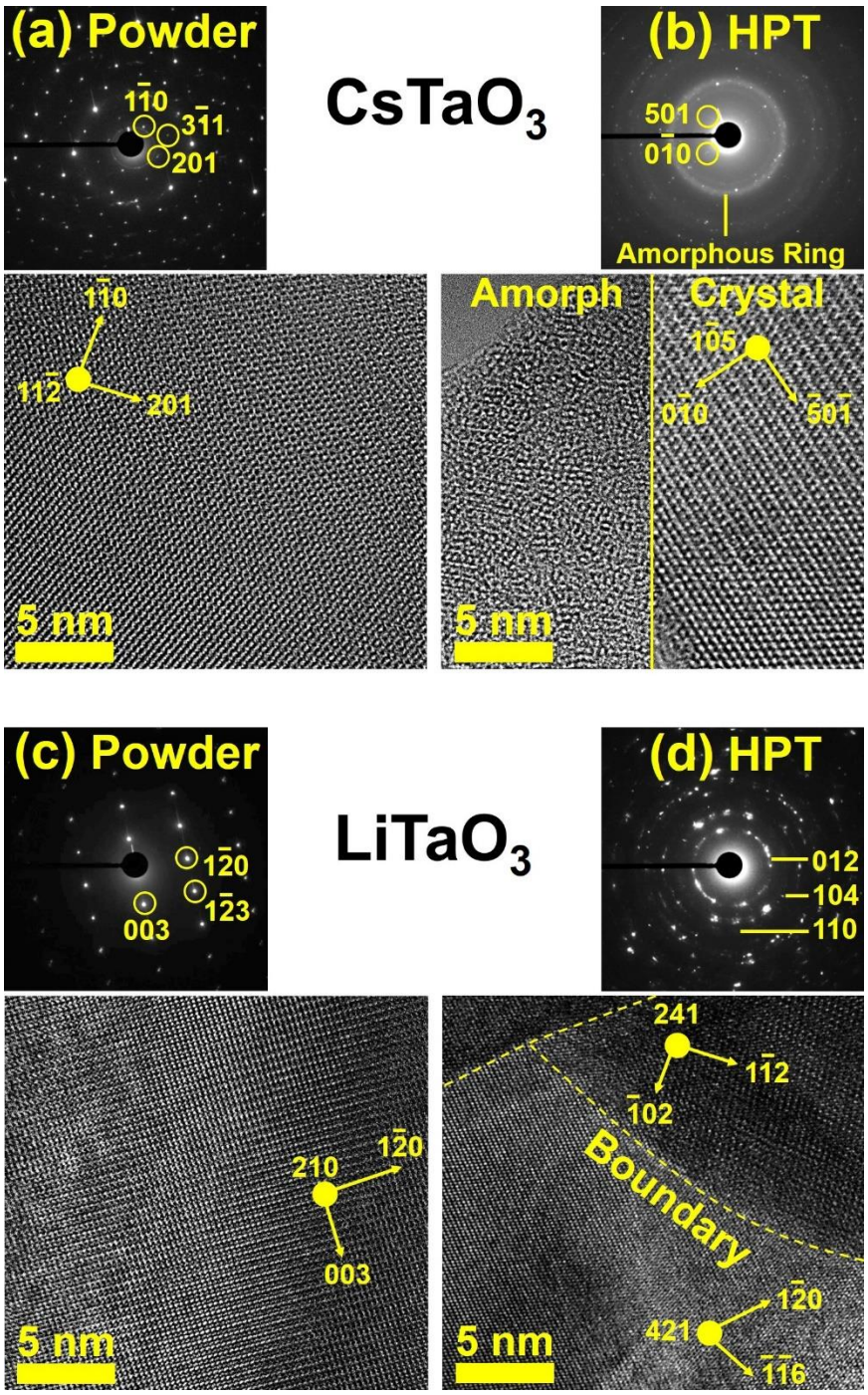

Figure 2. Reduction of crystalline size and amorphization in tantalate perovskites by severe straining. TEM high-resolution lattice images and SAED patterns for (a, b) $CsTaO_3$ and (c, d) $LiTaO_3$, where (a, b) correspond to powders and (c, d) correspond to HPT-processed samples.

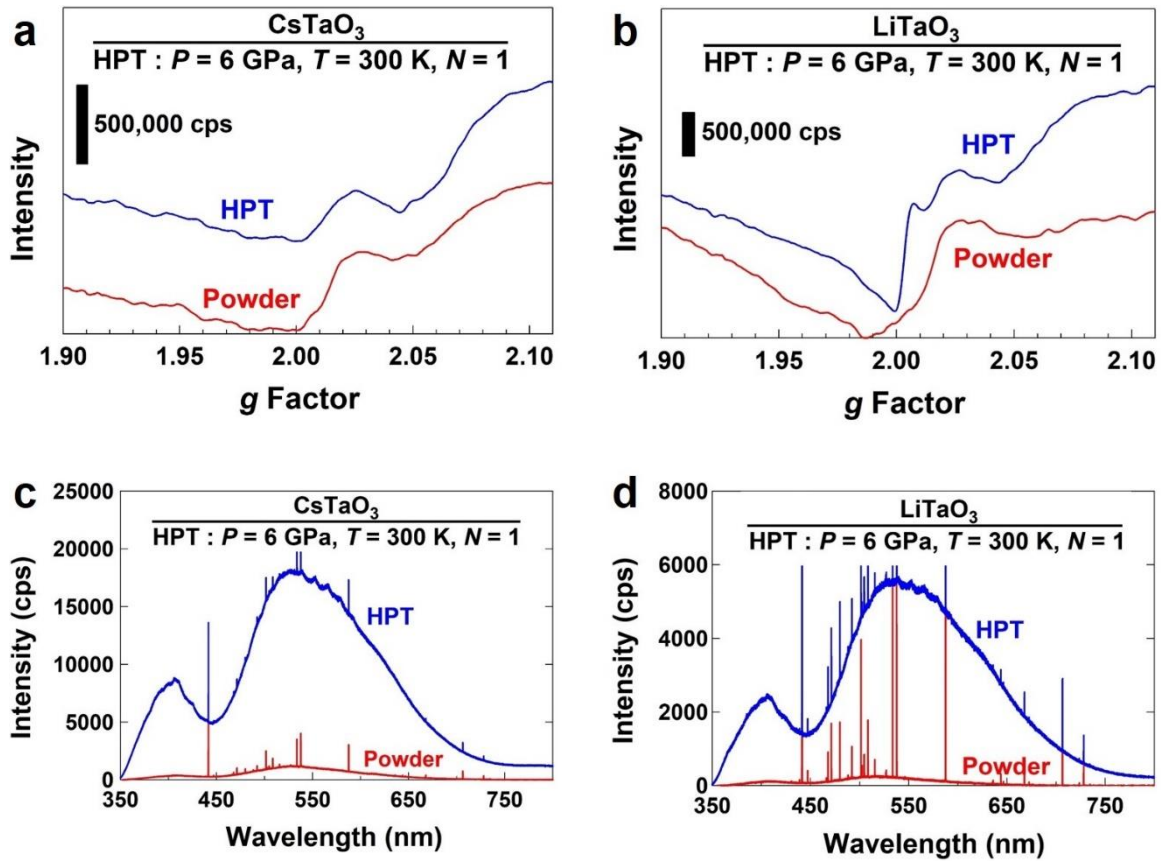

Figure 3. Formation of oxygen vacancies in tantalate perovskites by severe straining. (a, b) ESR spectra and (c, d) PL spectra for (a, c) $CsTaO_3$ and (b, d) $LiTaO_3$ before (powder) and after processing by HPT.

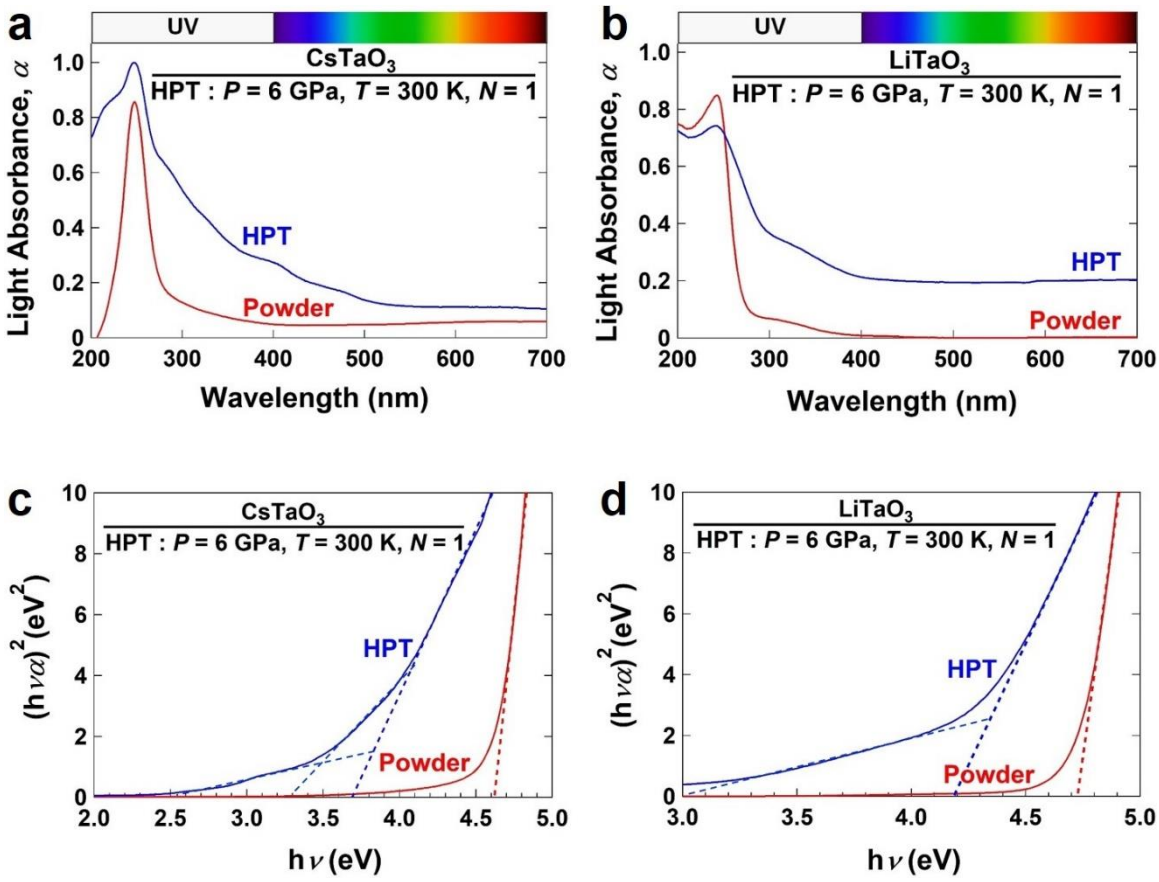

Figure 4. Enhanced light absorbance and bandgap narrowing in tantalate perovskites by severe straining. (a, b) UV-Vis reflectance spectra and (c, d) Kubelka-Munk plots for (a, c) $CsTaO_3$ and (b, d) $LiTaO_3$ before (powder) and after processing by HPT.

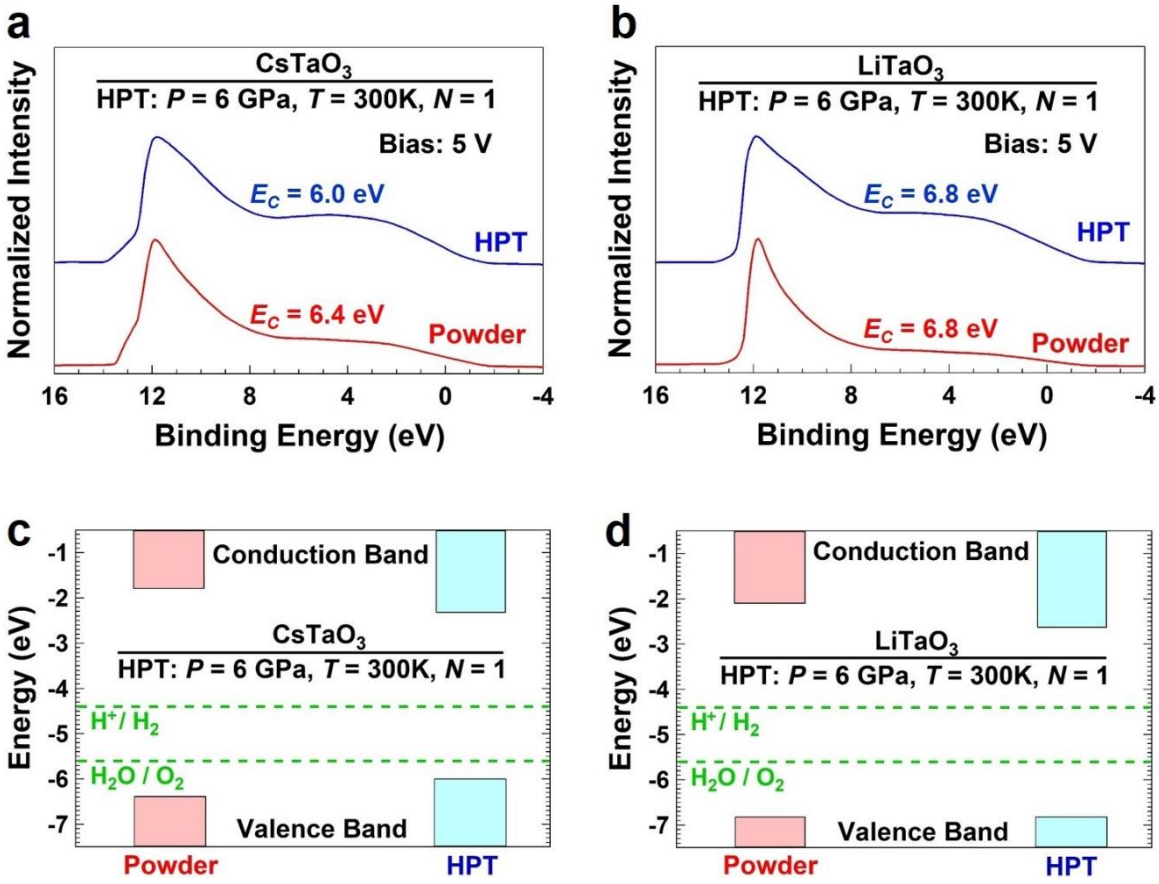

Figure 5. Changes in bandgap, valence band and conduction band energy levels in tantalate perovskites by severe straining. (a, b) UPS spectra and (c, d) band structure determined by UV-Vis reflectance spectroscopy and UPS for (a, c) $CsTaO_3$ and (b, d) $LiTaO_3$ before (powder) and after processing by HPT.

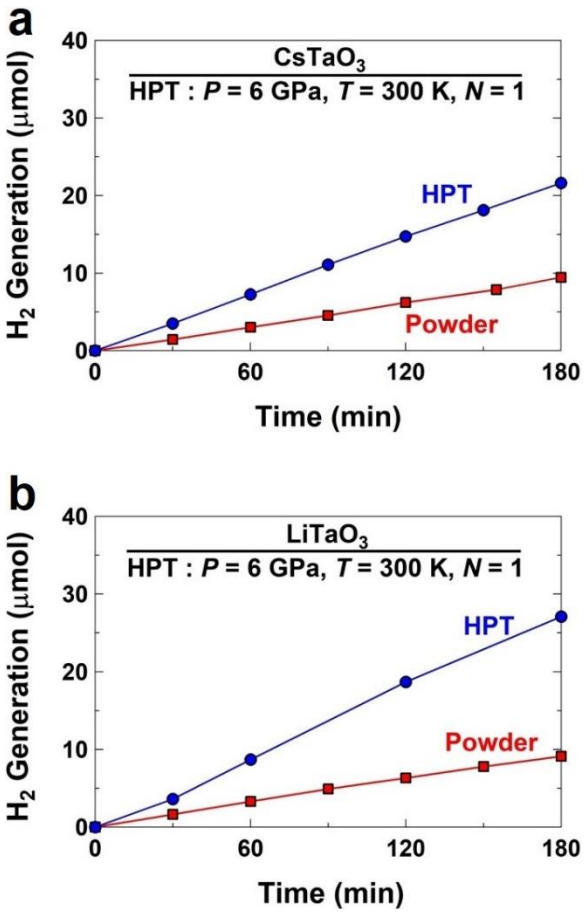

Figure 6. Enhancement of photocatalytic activity of tantalate perovskites by severe straining. Photocatalytic hydrogen production against exposure time under UV light for (a) $CsTaO_3$ and (b) $LiTaO_3$ before (powder) and after processing by HPT.

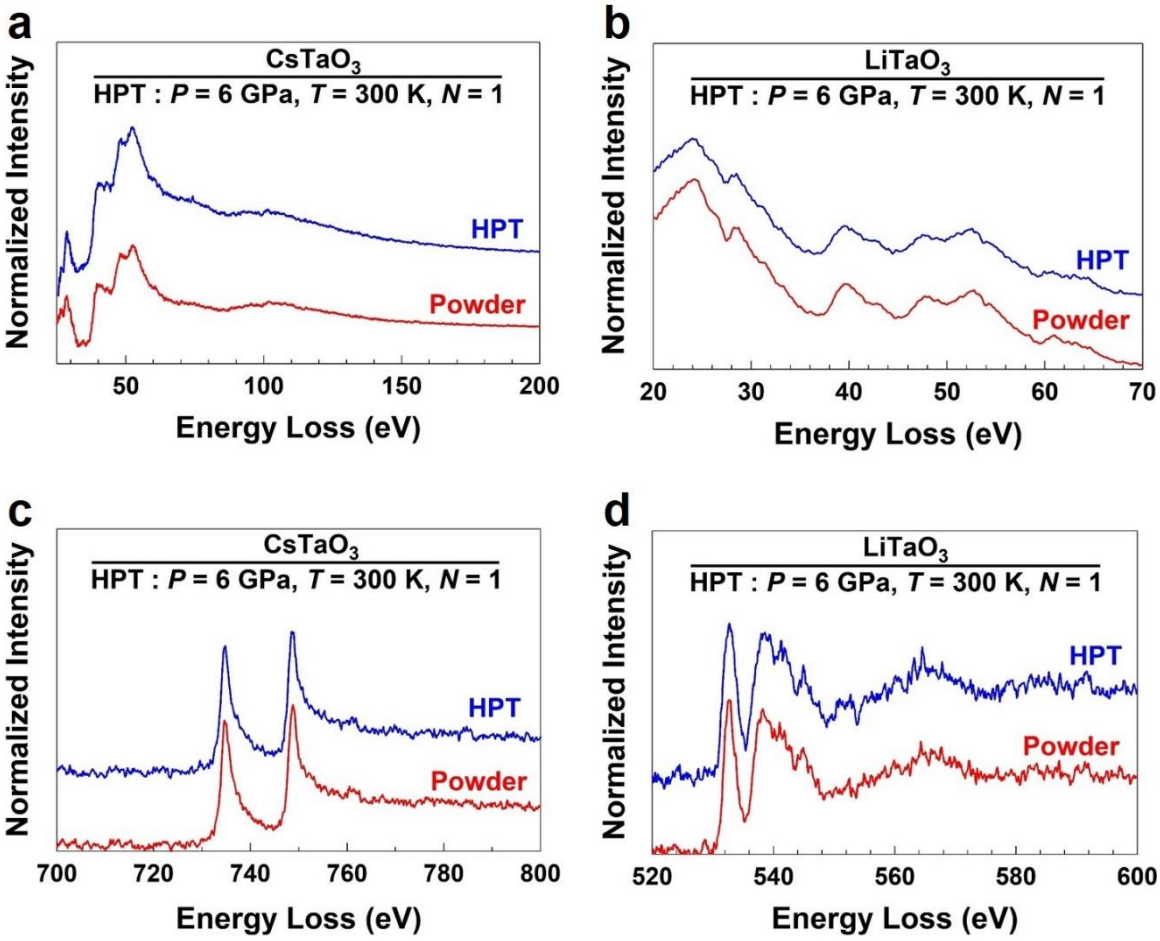

Figure A1. No significant change in EELS spectra of tantalate perovskites by severe straining. EELS (a, b) low-loss and (c, d) high-loss spectra for (a, c) $CsTaO_3$ and (b, d) $LiTaO_3$ before (powder) and after processing by HPT.

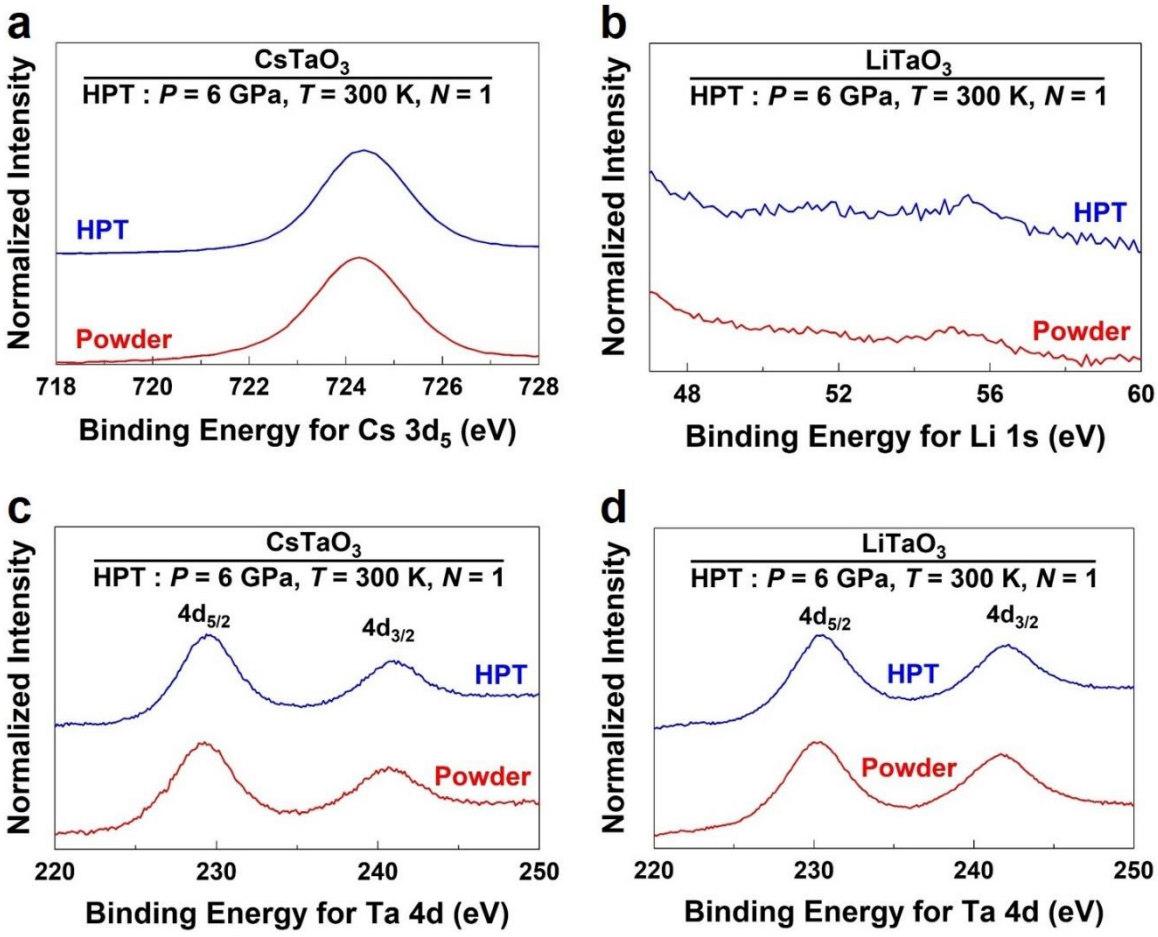

Figure A2. No significant change in XPS spectra of tantalate perovskites by severe straining. UPS spectra for (a) Cs $3d_5$, (b) Li 1s and (c, d) Ta $4d_{5/2}$ and Ta $4d_{3/2}$ for (a, c) $CsTaO_3$ and (b, d) $LiTaO_3$ before (powder) and after processing by HPT.